Spectroscopic Signatures of a Liouvillian Exceptional Spectral Phase in a Collective Spin

Rafael A. Molina

1 Instituto de Estructura de la Materia (IEM-CSIC), E-28006, Madrid, Spain

rafael.molina@csic.es

Abstract

Non-Hermitian degeneracies of Lindblad generators (Liouvillian exceptional points) can induce non-exponential relaxation and higher-order poles in dynamical response functions. A collective spin coupled to a polarized Markovian bath exhibits an *exceptional spectral phase* in which defective Liouvillian modes imprint super-Lorentzian features in frequency-resolved spectra. We compute the emission spectrum via the Liouvillian resolvent, identify symmetry-sector selection rules, and demonstrate that exceptional-point signatures are strongly state-dependent: they are suppressed in steady-state fluorescence yet become unambiguous for generic (infinite-temperature or random) initial states. Our results provide an experimentally accessible spectroscopic diagnostic of many-body Liouvillian exceptional phases and clarify when steady-state emission can (and cannot) reveal them.

Contents

arXiv:2602.01375v2 [quant-ph] 24 Feb 2026

1   Introduction

Exceptional points (EPs)—non-Hermitian degeneracies at which both eigenvalues and eigenvectors coalesce—have emerged as a unifying concept behind a broad range of critical phenomena in open and effective non-Hermitian systems. Formally, EPs are branch-point singularities of the resolvent and are naturally associated with Jordan blocks and non-exponential dynamics [1–5]. In condensed-matter systems they provide a powerful framework to engineer and classify quantum phase transitions and novel topological phases, enabling robust boundary phenomena rooted in the singular topology of the complex energy spectrum [6–13]. In optics and photonics they underpin striking effects such as enhanced sensitivity and chiral mode transfer, and have motivated extensive experimental and theoretical activity [14–16].

In quantum Markovian dynamics, the generator of evolution is the Liouvillian superoperator of a Lindblad master equation. Liouvillians are intrinsically non-Hermitian, and can host *Liouvillian exceptional points* (LEPs)—degeneracies in the Liouvillian spectrum where eigenmatrices coalesce [17]. LEPs have distinct features compared to EPs of effective non-Hermitian Hamiltonians, because the Liouvillian necessarily incorporates quantum noise and jump processes [17,18]. A growing body of work has developed both the mathematical characterization and the physical consequences of LEPs, including explicit constructions of LEPs of higher order and their imprint on coherence and spectral functions [19, 20], as well as recent reviews emphasizing dynamical phenomena such as chiral state transfer upon parametric encircling [21]. On the experimental side, postselected quantum-trajectory protocols have enabled the observation of EP physics in superconducting circuits [22], and related approaches have clarified how trajectory conditioning connects Hamiltonian and Liouvillian notions of EPs [18].

A central open question is *how* and *when* Liouvillian EP structure becomes visible in experimentally natural observables, in particular in frequency-resolved emission spectra. Unlike traditional Hermitian systems, the spectral behavior near EPs exhibits non-Lorentzian features, including super-Lorentzian line shapes, due to the enhanced non-orthogonality and spectral sensitivity inherent to these degeneracies. Hashemi *et al.* demonstrated that higher-order EPs result in power-law broadened responses surpassing Lorentzian limits, fundamentally shaping the emission profiles of such systems [23]. Extending this, Bid and Schomerus showed how these features persist even beyond the EP itself, emphasizing the non-trivial topology of the system's spectrum [24]. Simonson *et al.* further revealed that quantum noise near EPs leads to a hybrid of Lorentzian and super-Lorentzian spectral features, which can enhance or suppress emission depending on system parameters [25]. Kullig *et al.* analytically connected these spectral anomalies to a generalized Petermann factor, providing a deeper theoretical basis for emission scaling in EP-governed regimes [26]. Together, these studies frame the emission spectrum in the exceptional phase not merely as broadened or shifted, but as a signature of underlying non-Hermitian singularities.

In this work we address this question in the setting of a dissipative collective spin coupled

to a polarized Markovian bath. This model exhibits an *exceptional spectral phase* (ESP) in which, in the thermodynamic limit, an extensive region of the Liouvillian spectrum becomes populated exclusively by second-order EPs, separated from a normal spectral phase by a critical line where the spectral density diverges [27]. By an exceptional spectral phase (ESP) we mean a regime in which, in the thermodynamic limit, a finite fraction of the Liouvillian spectrum becomes defective, forming an extensive set of second-order exceptional points rather than isolated degeneracies. The same general framework also connects naturally to symmetry-resolved Lindblad dynamics and trajectory physics, where strong symmetries can induce sector selection and dissipative freezing at the level of individual quantum trajectories [28].

Here we compute the emission spectrum from the Liouvillian resolvent and demonstrate a state-dependent visibility of exceptional structure. While LEPs are a property of the Liouvillian itself, their spectroscopic signatures depend on the overlap between the emission channel and the defective subspace. We show that steady-state fluorescence can strongly suppress the second-order (super-Lorentzian) contribution even deep in the ESP, whereas spectra sourced from generic initial states (infinite temperature or random full-rank states) reveal a pronounced and statistically significant higher-order pole contribution. This establishes a practical spectroscopic diagnostic of Liouvillian exceptional phases and clarifies why steady-state emission may fail to reveal them even when the underlying Liouvillian is defective.

2 Model

We consider a collective spin of length j with Hamiltonian

$$H = -hJ_z, \tag{1}$$

and Markovian open-system dynamics described by a Lindblad master equation $\dot{\rho} = \mathcal{L}\rho$ [29, 30],

$$\mathcal{L}\rho = -i[H,\rho] + \sum_{\ell \in \{0,+,-\}} \left(L_\ell \rho L_\ell^\dagger - \tfrac{1}{2}\{L_\ell^\dagger L_\ell, \rho\} \right). \tag{2}$$

The jump operators are

$$L_0 = \sqrt{\Gamma_0/j}\, J_z, \qquad L_\pm = \sqrt{\Gamma(1\mp p)/(2j)}\, J_\pm, \tag{3}$$

where J_α are collective $\mathfrak{su}(2)$ generators, Γ and Γ_0 set the dissipative rates, and $p \in [-1,1]$ controls the polarization of the environment. This model was first studied by Riberio and Prosen as an example of exactly solvable many-body Liouvillian [31]. In Appendix A we discuss the vectorized form of the Liouvillian, the symmtries and the complex spectrum of the model.

2.1 Physical realizations

Equation (2) describes a broad class of collective open quantum systems. A paradigmatic realization is an ensemble of $N = 2j$ identical two-level atoms restricted to the fully symmetric Dicke manifold, where $J_\pm = \sum_{k=1}^N \sigma_\pm^{(k)}$ and $J_z = \tfrac{1}{2}\sum_{k=1}^N \sigma_z^{(k)}$. In this context, the operators $L_\pm$ describe collective spontaneous emission and absorption, while L_0 represents collective dephasing due to, e.g., elastic light scattering or fluctuating fields [32–34]. The bath polarization parameter p interpolates between unbiased decay ($p = 0$), corresponding to an infinite-temperature environment, and a fully polarized bath ($p = \pm 1$), where either emission or absorption is suppressed and the dynamics becomes strongly directional. For intermediate values of p and taking into account detailed balance it is possible to relate the jump operators to a bath with inverse temperature $\beta = \frac{1}{h}ln(\frac{1-p}{1+p})$ [27].

Closely related Lindblad structures also arise in solid-state settings. For example, a localized magnetic moment or quantum dot spin coupled to a spin-polarized electronic reservoir experiences incoherent spin-flip processes whose rates depend on the reservoir polarization, together with longitudinal dephasing due to elastic scattering [35, 36]. In this interpretation, $J_\pm$ generate collective (or effective) spin flips and p encodes the degree of spin polarization of the leads or substrate. Such models are directly relevant to scanning tunneling microscopy experiments on single magnetic atoms and engineered nanostructures, where spin dynamics is probed via frequency-resolved noise or ESR-type measurements [37].

2.2 Emission spectrum and physical meaning

We define the emission spectrum associated with collective spin lowering as

$$S(\omega) = \lim_{t \to \infty} \frac{1}{\pi} \operatorname{Re} \int_0^\infty d\tau \, e^{i\omega\tau} \langle J_+(t) J_-(t+\tau) \rangle, \tag{4}$$

where the expectation value is taken with respect to the system density matrix at time t. As mentioned earlier, in quantum-optical realizations, J_- plays the role of a collective dipole operator: for an ensemble of N identical two-level emitters in the symmetric manifold, one has $J_- = \sum_{k=1}^N \sigma_-^{(k)}$ and $J_+ = J_-^\dagger$. In the far field, the positive-frequency component of the radiated electric field is proportional to J_- (up to geometry- and polarization-dependent factors), so that $S(\omega)$ corresponds to the frequency-resolved power spectrum of collective fluorescence (resonance fluorescence in the driven case) [32–34, 38]. In this sense, $S(\omega)$ is an experimentally accessible observable in platforms ranging from cold-atom ensembles and superradiant emitters to cavity-QED implementations of collective decay [32, 33].

The same correlator has a natural interpretation in solid-state realizations where a localized spin couples to itinerant electrons or to a detector. For instance, in ESR-STM measurements of a single magnetic atom on a surface, the detected signal is sensitive to transverse spin dynamics at the Larmor frequency and is commonly expressed in terms of spin correlation functions closely related to $\langle S_+(t) S_-(t+\tau) \rangle$ (or equivalently to the corresponding dynamical susceptibility) [37, 39]. In this context, $S(\omega)$ captures the spectral content of spin-flip fluctuations and can be interpreted as a "spin-emission" (or spin-noise) spectrum of the localized moment.[1]

2.3 Quantum regression and resolvent form

Using the quantum regression theorem (QRT) [34], Eq. (4) becomes

$$S(\omega) = \lim_{t \to \infty} \frac{1}{\pi} \operatorname{Re} \int_0^\infty d\tau \, e^{i\omega\tau} \operatorname{Tr} \left[J_- e^{\mathcal{L}\tau} \big(\rho(t) J_+ \big) \right]. \tag{5}$$

For a unique steady state $\rho(t \to \infty) = \rho_{\rm ss}$, Eq. (5) can be written in a resolvent form

$$S(\omega) = \frac{1}{\pi} \operatorname{Re} \operatorname{Tr} \left[J_- \big(i\omega - \mathcal{L} \big)^{-1} \big(\rho_{\rm ss} J_+ \big) \right], \tag{6}$$

which makes explicit that $S(\omega)$ probes poles of the Liouvillian resolvent. In particular, defective Liouvillian modes (exceptional points) generate higher-order poles and can therefore produce non-Lorentzian "super-Lorentzian" features in $S(\omega)$, provided the source operator $\rho_{\rm ss} J_+$ has nonzero overlap with the corresponding Jordan subspace.

---

[1]The precise proportionality between the measured current noise / conductance features and spin correlators depends on the microscopic tunneling Hamiltonian and detection protocol, but transverse spin spectra are the central theoretical object in both spin-noise and ESR-STM descriptions [37, 39].

2.4 Sector selection rule

Because ρ_{ss} is diagonal in the J_z basis, the source operator $X \equiv \rho_{ss} J_+$ has matrix elements only of the form $|m\rangle\langle m-1|$, i.e. it lies entirely in the $M = 1$ block. Since $\mathcal{L}$ preserves M, only Liouvillian modes in sector $M = 1$ contribute to $S(\omega)$.

3 Exceptional-Point Signatures and State-Dependent Visibility

3.1 Generalized spectra for arbitrary initial states

To probe Liouvillian structure beyond steady-state fluorescence, we also consider the spectrum sourced by an arbitrary state ρ_0,

$$S(\omega; \rho_0) = \frac{1}{\pi} \operatorname{Re} \mathbf{Tr}\left[J_m \left(i\omega - \mathcal{L} \right)^{-1} \left(\rho_0 J_p \right) \right], \tag{7}$$

including $\rho_0 = \mathbb{I}/d$ (infinite temperature) and random full-rank states.

3.2 Lorentzian vs super-Lorentzian discrimination

Equation (6) shows that the emission spectrum probes the resolvent $(i\omega - \mathcal{L})^{-1}$ of the Liouvillian. If $\mathcal{L}$ is diagonalizable, isolated eigenmodes contribute simple poles of the form $(\gamma_\mu + i(\omega - \omega_\mu))^{-1}$, yielding Lorentzian line shapes. By contrast, if $mathcalL$ possesses a defective eigenvalue λ_μ associated with a Jordan block of size two, the resolvent develops a second-order pole $(i\omega - \lambda_\mu)^{-2}$, producing a qualitatively distinct "super-Lorentzian" contribution [1, 5, 23, 25]. Such higher-order poles are the direct spectral signature of Liouvillian exceptional points. More details about the derivation can be found in the Appendix.

Motivated by this structure, we analyze the emission spectrum near its dominant peak using two nested phenomenological models. Model A (Lorentzian) assumes a single simple pole,

$$S_A(\omega) = \frac{a}{(\omega - \omega_0)^2 + \gamma^2} + c, \tag{8}$$

while Model B (Lorentzian + super-Lorentzian) includes an additional second-order pole,

$$S_B(\omega) = \frac{a}{(\omega - \omega_0)^2 + \gamma^2} + \frac{b\left[\gamma^2 - (\omega - \omega_0)^2\right]}{\left[(\omega - \omega_0)^2 + \gamma^2\right]^2} + c. \tag{9}$$

Model B reduces continuously to Model A for $b = 0$ and therefore provides a minimal extension that captures the effect of a size-two Jordan block in the Liouvillian spectrum. The parameter b quantifies the relative weight of the second-order pole contribution.

To characterize the importance of the exceptional-point component, we define the EP weight

$$r \equiv \frac{|b|}{|a| + |b|}, \tag{10}$$

which measures the fraction of spectral weight associated with the super-Lorentzian term. While r is not an order parameter in a strict sense, a nonzero value signals a resolvent contribution that cannot be generated by diagonalizable Liouvillian modes alone.

Because Model B contains Model A as a special case, visual comparison of fits is insufficient to assess the statistical relevance of the additional parameter. We therefore employ information-criterion-based model selection. Specifically, we compute the Bayesian information criterion (BIC),

$$\text{BIC} = k \ln N + N \ln(\text{RSS}/N), \tag{11}$$

where k is the number of fit parameters, N the number of data points, and RSS the residual sum of squares [40, 41]. Negative values of $\Delta\text{BIC} = \text{BIC}_B - \text{BIC}_A$ indicate that the super-Lorentzian model is statistically favored despite its larger parameter count. This criterion provides a robust, quantitative discriminator between ordinary Lorentzian spectra and genuine exceptional-point-induced line shapes.

4 Numerical Results

We now present numerical results for the emission spectrum and its exceptional-point diagnostics in the collective spin model (2)–(3). Numerically, the resolvent is evaluated by explicit construction and inversion of the Liouvillian matrix in the relevant symmetry sector, and fits are performed in a window around the dominant peak. Unless otherwise stated, we fix $h = 1$ and scale the dissipative rates with system size as $\Gamma \propto j^0$, which yields a nontrivial thermodynamic limit [27]. All spectra are computed from the Liouvillian resolvent (6) and analyzed using the Lorentzian and super-Lorentzian models introduced in Sec. III.

4.1 Steady-state versus generic-state emission

Figures 1a and 1b compare the emission spectrum obtained from the steady state ρ_{ss} with that obtained from a generic initial random state and an infinite-temperature state $\rho_0 = \mathbb{I}/d$, for identical Liouvillian parameters with two values of the polarization parameter $p = 0.2$ and $p = 0.9$. In both cases the spectrum exhibits a dominant peak at $\omega = h$, whose width and position are controlled by the decay rates and coherent precession frequency.

Figure 1 illustrates how the structure of the emission spectrum evolves as the incoherent pumping strength bath polarization is increased. For moderate pumping ($p = 0.2$), shown in the upper panel, the spectra obtained from the steady state, the infinite-temperature state, and a random reference state are all well captured by a single Lorentzian profile, although with small deviations in the infinite temperature and random initial states. This indicates that the Liouvillian spectrum is dominated by well-isolated decay modes, and that the spectral response is largely insensitive to the choice of initial state.

In contrast, for strong pumping ($p = 0.9$), shown in the lower panel, the infinite-temperature and random-state spectra exhibit pronounced deviations from a single-Lorentzian form and are better described by a model that includes an additional superlorentzian contribution. This qualitative change is absent in the steady state which remain comparatively smooth. The enhanced sensitivity of the steady-state response at large p is consistent with the appearance of near-degenerate Liouvillian modes and the spectral crowding discussed in the context of Fig. 3. Together, these results highlight how collective dissipation and Liouvillian spectral structure manifest directly in experimentally accessible frequency-domain observables. For both values of the parameter p the infinite temperature and the random initial states have almost the same emission spectrum.

Despite the presence of an exceptional spectral phase (ESP) in the Liouvillian spectrum, the steady-state emission is accurately described by a purely Lorentzian line shape. Information-criterion analysis strongly favors the Lorentzian model, with large positive values of ΔBIC, and the extracted EP weight r remains close to zero. By contrast, for the infinite-temperature state and the random states the Lorentzian model fails to capture the line shape: the inclusion of a super-Lorentzian term yields a dramatic reduction of the residual error and is overwhelmingly favored by both AIC and BIC. The corresponding EP weight reaches values of order $r \sim 10^{-1}$, providing clear evidence for a second-order pole contribution associated with a defective Liouvillian mode.
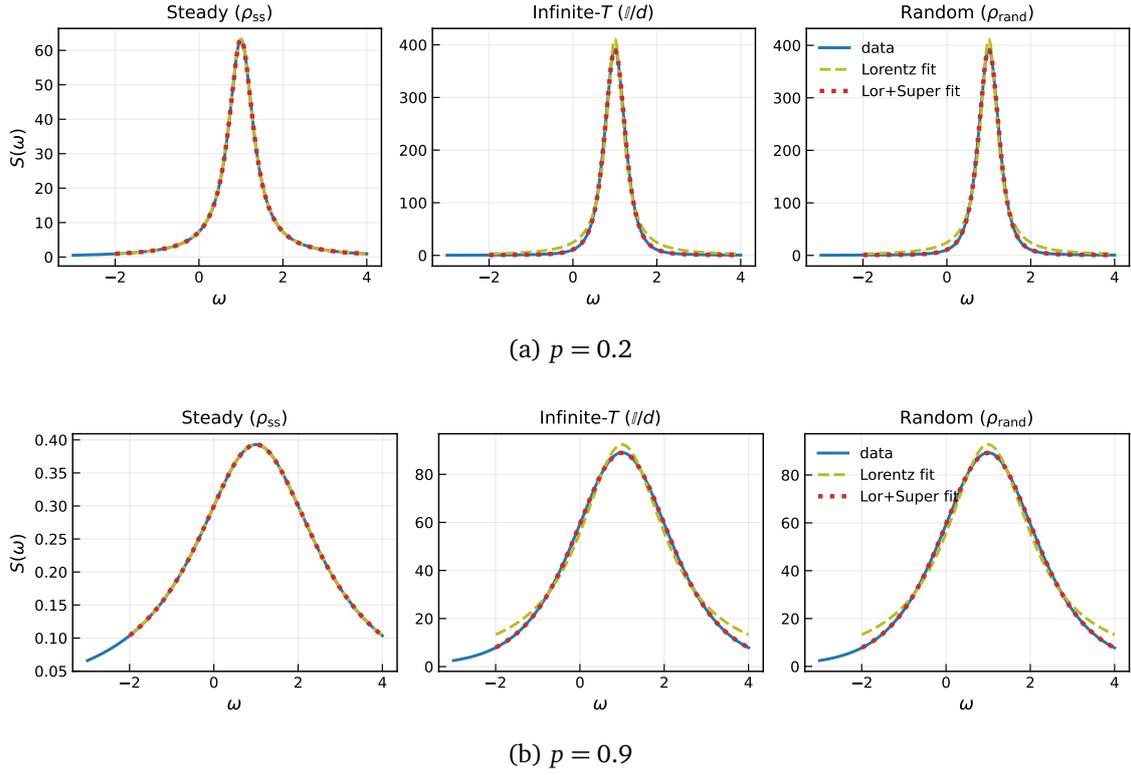
(a) $p = 0.2$

(b) $p = 0.9$

Figure 1: Emission spectra $S(\omega)$ computed from the Liouvillian resolvent for two representative values of the polarization paraemeter p. In each panel, spectra are shown for the steady state ρ_{ss}, the infinite-temperature state $\rho_\infty = \mathbb{1}/d$, and a random reference state, together with fits to a single Lorentzian and to a Lorentzian-plus-superlorentzian model. For weak pumping ($p = 0.2$, upper panel), Steady state spectra are well described by a single lorentzian for both values of p, indicating isolated Liouvillian resonances. However at stronger pumping ($p = 0.9$, lower panel), the infinite-temperature and random-state spectra develop clearer deviations from a single-lorentzian lineshape and are well fitted by a Lorentzian plus super-lorentzian lineshape. This behavior reflects the increasing role of collective and near-degenerate Liouvillian modes at large p.

This striking contrast demonstrates that exceptional points are a property of the Liouvillian generator, but their spectroscopic visibility depends crucially on the overlap between the emission channel and the defective subspace. In the present model, the steady state becomes increasingly polarized as $p \to 1$, which suppresses the source operator $\rho_{ss} J_+$ in the $M = 1$ sector and effectively filters out the exceptional contribution, even though the Liouvillian itself remains defective.

4.2 Exceptional-point diagnostics versus bath polarization

To characterize the emergence of exceptional behavior systematically, we analyze the EP diagnostics as a function of bath polarization p and system size j. The lower panel Figure 2 shows the EP weight $r(p)$ (right) and the model-selection indicator $\Delta\mathrm{BIC}(p)$ (left) extracted from spectra computed with infinite-temperature and steady-state sources.

For generic initial states, both diagnostics reveal a sharp crossover as p is increased: $r(p)$ grows rapidly from zero and $\Delta\mathrm{BIC}$ becomes strongly negative, signaling the onset of a statistically significant super-Lorentzian contribution. As the system size increases, this crossover
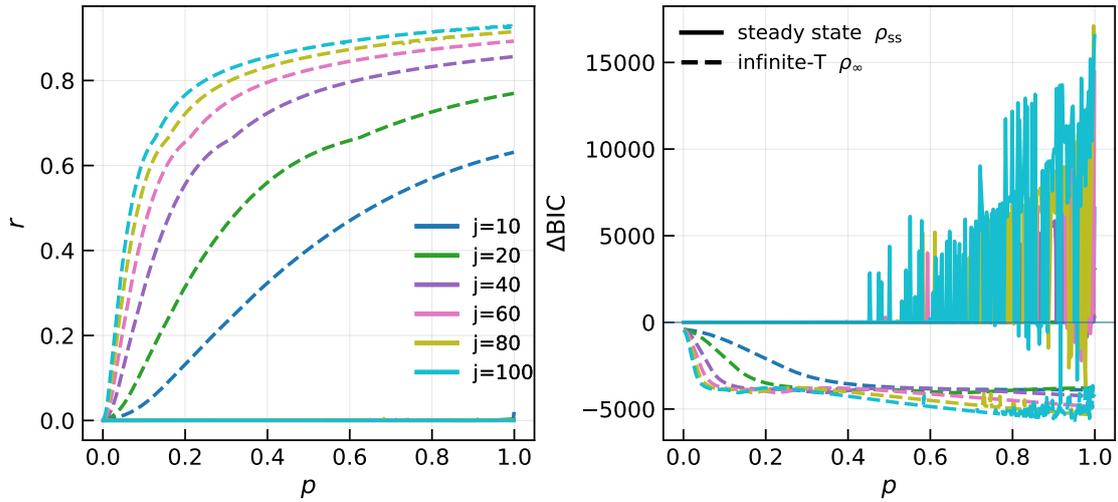
Figure 2: **Emission spectra and Liouvillian exceptional-point diagnostics.** (a) Steady-state emission spectrum $S(\omega)$ and Lorentzian fit. (b) Spectrum $S(\omega; \rho_0)$ for $\rho_0 = \mathbb{I}/d$ with Lorentzian and Lorentzian+super-Lorentzian fits. (lower panel) Extracted EP weight r and information-criterion difference ΔBIC.

becomes increasingly sharp and shifts toward smaller values of p, consistent with the approach to the thermodynamic exceptional spectral phase identified in Ref. [27]. By contrast, the same diagnostics applied to steady-state spectra remain near their Lorentzian values for all p, reflecting the steady-state filtering discussed above.

This analysis clarifies that the EP weight r is not an order parameter, but rather a measure of spectral dominance: it quantifies when defective modes control the observable response, not merely when they exist. Consequently, the boundary of the exceptional spectral phase is more robustly identified by information-criterion diagnostics than by the maximum of $r(p)$.

5   Discussion and Outlook

We have shown that exceptional points of a Liouvillian generator can leave clear and quantifiable fingerprints in emission spectra, provided that the emission channel has sufficient overlap with the defective subspace. In a dissipative collective spin model exhibiting an exceptional spectral phase, we identified super-Lorentzian line shapes as the direct manifestation of second-order poles in the Liouvillian resolvent. Crucially, we demonstrated that the visibility of these signatures is strongly state-dependent: while generic initial states reveal the exceptional structure through statistically significant deviations from Lorentzian behavior, steady-state emission can remain essentially blind to it due to polarization-induced filtering.

This state-dependent visibility clarifies an important conceptual point. Exceptional points are properties of the dynamical generator, not of a particular observable or preparation, and their experimental detectability depends on how the system is probed. In the present model, the steady state suppresses the source operator that couples to the defective modes, even deep inside the exceptional spectral phase. Our results therefore explain why steady-state fluorescence measurements may fail to detect Liouvillian exceptional points, and why transient, quenched, or otherwise nonequilibrium protocols are often essential.

The spectroscopic diagnostics introduced here—super-Lorentzian fitting combined with information-criterion-based model selection—provide a practical and broadly applicable toolkit

for identifying Liouvillian exceptional behavior. Because these diagnostics rely only on frequency-resolved correlation functions, they are directly relevant to a wide range of experimental platforms, including collective atomic ensembles, cavity and circuit QED systems, and nanoscale magnetic structures probed by spin-resolved spectroscopy. In particular, our analysis suggests that measurements performed after a quench or from engineered mixed states may be more sensitive to exceptional physics than steady-state fluorescence alone.

Several natural extensions follow from this work. First, it would be interesting to generalize the present analysis to higher-order Liouvillian exceptional points, where the resolvent contains poles of order three or higher and the resulting spectral line shapes are expected to be even more distinctive. Second, the role of individual quantum trajectories merits further investigation: trajectory-conditioned dynamics are known to exhibit exceptional points even when the unconditional Liouvillian does not, and conversely may provide enhanced sensitivity to defective modes. Finally, extending these ideas to spatially extended or multimode systems could establish a direct link between exceptional spectral phases and transport or many-body localization phenomena in open quantum matter.

More broadly, our results highlight emission spectroscopy as a powerful probe of the non-Hermitian structure of open quantum systems. By explicitly connecting Liouvillian exceptional points to observable spectral features, we provide a concrete route for exploring non-Hermitian criticality in realistic quantum platforms.

A   Liouville-space formulation and weak symmetry

A.1   Vectorization of the Liouvillian

To analyze the spectral properties of the Liouvillian appearing in Eqs. (1)–(3) of the main text, it is convenient to work in Liouville space by vectorizing the density matrix [42]. We adopt the standard column-stacking convention,

$$\text{vec}(\rho) = \sum_{m,n} \rho_{mn} |m\rangle \otimes |n\rangle, \tag{A.1}$$

under which operator multiplication maps as

$$\text{vec}(A\rho B) = (A \otimes B^{\mathsf{T}}) \text{vec}(\rho). \tag{A.2}$$

Using this representation, the Lindblad generator

$$\mathcal{L}\rho = -i[H,\rho] + \sum_{\ell} \left(L_\ell \rho L_\ell^\dagger - \tfrac{1}{2}\{L_\ell^\dagger L_\ell, \rho\} \right) \tag{A.3}$$

is mapped onto a non-Hermitian superoperator matrix

$$\mathcal{L} = -i\left(H \otimes \mathbb{I} - \mathbb{I} \otimes H^{\mathsf{T}}\right) + \sum_{\ell} \left(L_\ell \otimes L_\ell^* - \tfrac{1}{2}L_\ell^\dagger L_\ell \otimes \mathbb{I} - \tfrac{1}{2}\mathbb{I} \otimes (L_\ell^\dagger L_\ell)^{\mathsf{T}} \right), \tag{A.4}$$

acting on the Liouville-space vector $|\rho\rangle\rangle = \text{vec}(\rho)$. The Liouvillian spectrum is obtained from

$$\mathcal{L}|\rho_\mu\rangle\rangle = \lambda_\mu |\rho_\mu\rangle\rangle, \tag{A.5}$$

where the eigenvalues λ_μ are generally complex and may form nontrivial Jordan blocks.

A.2   Explicit vectorized Liouvillian for the collective-spin model

For completeness, we write the Liouvillian matrix $\mathcal{L}$ explicitly in the vectorized representation for the model of Eqs. (2)–(3). Following Refs. [27], we map an $N \times N$ density matrix $\rho_{\alpha,\beta}$ (with $N = 2j+1$) to a vector $|\alpha, \beta\rangle\rangle$ in a Hilbert space of dimension N^2. Left and right multiplications by collective-spin operators are represented as

$$J\rho \mapsto (J \otimes \mathbb{I})|\rho\rangle\rangle \equiv K_1 |\rho\rangle\rangle, \qquad \rho J \mapsto (\mathbb{I} \otimes J^{\mathsf{T}})|\rho\rangle\rangle \equiv K_2 |\rho\rangle\rangle, \qquad (A.6)$$

so that $K_{1\alpha}$ and $K_{2\alpha}$ ($\alpha = x, y, z$) form two commuting spin-j $\mathfrak{su}(2)$ algebras acting on the left and right indices, respectively.

Using $H = -hJ_z$ and the jumps $L_0 = \sqrt{\Gamma_0/j}\, J_z$ and $L_\pm = \sqrt{\Gamma(1 \mp p)/(2j)}\, J_\pm$, the Liouvillian superoperator $\mathcal{L}$ becomes an explicit non-Hermitian operator on Liouville space:

$$\mathcal{L} = -\Gamma(j+1) + ih(K_{1z} - K_{2z}) + \frac{\Gamma}{j} K_{1z} K_{2z} + \frac{\Gamma - \Gamma_0}{2j}(K_{1z} - K_{2z})^2$$

$$- \frac{\Gamma}{j}\frac{p}{2}(K_{1z} + K_{2z}) + \frac{\Gamma}{j}\frac{1-p}{2} K_{1+} K_{2+} + \frac{\Gamma}{j}\frac{1+p}{2} K_{1-} K_{2-}. \qquad (A.7)$$

Equation (A.7) is the form used in Ref. [27] (their Eq. (4)), expressed in our notation. The z component

$$K_z \equiv K_{1z} - K_{2z} \qquad (A.8)$$

commutes with $\mathcal{L}$, $[\mathcal{L}, K_z] = 0$, and thus generates a weak symmetry that decomposes Liouville space into independent sectors labeled by $M \in \{-2j, -2j+1, \ldots, 2j\}$, corresponding to fixed eigenvalues of K_z [27, 28, 43]. The term proportional to Γ_0 produces a sector-dependent real shift, since $(K_{1z} - K_{2z})$ has fixed eigenvalue M within a given weak-symmetry block.

A.3   Liouvillian spectrum and near-degeneracies

Using the vectorized representation of the master equation introduced above, the full Liouvillian superoperator can be constructed explicitly and diagonalized numerically for moderate system sizes. Figure 3 shows the resulting Liouvillian spectrum for a collective spin with $j = 20$, plotted in the complex plane for several representative values of the bath polarization parameter p.

For no bath polarization ($p = 0$), the spectrum is well separated, with no visible clustering of eigenvalues. As p is increased, groups of eigenvalues approach each other in the complex plane in the region close to the steady state, these nearly degenerate region becomes larger for higher values of $|p|$ and is separated from the rest of the spectrum by a region of high density of eigenvalues [27, 44]. To highlight this behavior, eigenvalues that have at least one neighbor closer than $|\Delta\lambda| < 10^{-6}$ are marked in red. These near-degeneracies provide a clear numerical signature of spectral coalescence in the Liouvillian, consistent with the behavior expected in the vicinity of exceptional points in non-Hermitian generators. Rubio-Garcia *et al.* [27] demonstrated that in the Thermodynamic Limit $j \to \infty$ the eigenvalues really coalescence in pairs forming what they called an exceptional spectral phase separated with the normal phase of non-degenerate eigenvalues by a Liouvillian spectral phase transition with a divergent density of states, which is analogous to the excited state phase transitions of closed quantum systems [45].

A.4   Sector selection by emission observables

The emission spectrum studied in the main text involves the source operator
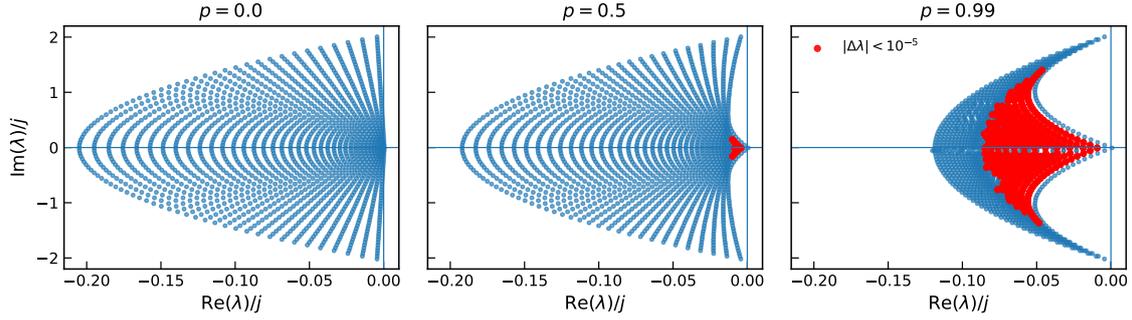
$$X = \rho J_+, \qquad (A.9)$$

Figure 3: Liouvillian spectrum for a collective spin system with $j = 20$, obtained by explicit vectorization of the master equation and direct diagonalization of the Liouvillian superoperator. The real and imaginary parts of the eigenvalues λ are shown (rescaled by j) for three representative values of the incoherent pumping parameter: $p = 0$, $p = 0.5$, and $p = 0.99$. All eigenvalues are plotted as black points, while eigenvalues that have at least one neighbor in the complex plane closer than $|\Delta\lambda| < 10^{-6}$ are highlighted in red. The latter provide a numerical diagnostic for near-degeneracies of the Liouvillian spectrum, consistent with the emergence of exceptional-point–like behavior as p is increased. Parameters are $h = 1$, $\Gamma = 0.1$, and $\Gamma_0 = 0$.

which in Liouville space contains only basis elements of the form $|m\rangle\langle m-1|$. These operators belong exclusively to the sector $M = 1$. Since the Liouvillian does not couple different M sectors, only the block $\mathcal{L}^{(M=1)}$ contributes to the resolvent expression for the emission spectrum.

This sector selection explains why exceptional points present in other symmetry sectors do not influence the observed spectrum, and why the visibility of exceptional behavior depends sensitively on the structure of the source state ρ. In particular, steady states that suppress the relevant sector components can effectively filter out exceptional contributions even when the Liouvillian itself remains defective.

A.5 Super-Lorentzian line shape from a Jordan-block resolvent

In this section we show explicitly why a *defective* Liouvillian (Jordan block) produces a "super-Lorentzian" contribution to the emission spectrum. We start from the resolvent form of the spectrum in the steady state,

$$S(\omega) = \frac{1}{\pi} \, \Re \, \mathbf{Tr} \left[J_- \, (i\omega - \mathcal{L})^{-1} \left(\rho_{ss} J_+ \right) \right], \tag{A.10}$$

and use the spectral structure of $(i\omega - \mathcal{L})^{-1}$ near an exceptional point.

Jordan block and resolvent. Consider an invariant subspace where $\mathcal{L}$ has a size-two Jordan block at eigenvalue λ_0,

$$\mathcal{L}\big|_{\text{sub}} = \lambda_0 \, \mathbb{I} + N, \qquad N = \begin{pmatrix} 0 & 1 \\ 0 & 0 \end{pmatrix}, \qquad N^2 = 0. \tag{A.11}$$

Then, for $z \equiv i\omega$, the resolvent restricted to this subspace can be inverted exactly:

$$
\begin{aligned}
(z - \mathcal{L})^{-1} &= \left[(z - \lambda_0)\mathbb{I} - N \right]^{-1} \\
&= \frac{1}{z - \lambda_0} \left[\mathbb{I} - \frac{N}{z - \lambda_0} \right]^{-1} = \frac{1}{z - \lambda_0} \left[\mathbb{I} + \frac{N}{z - \lambda_0} \right] \\
&= \frac{\mathbb{I}}{z - \lambda_0} + \frac{N}{(z - \lambda_0)^2}.
\end{aligned}
\tag{A.12}
$$

Equation (A.12) is the defining analytic signature of a Jordan block: a *second-order pole* at $z = \lambda_0$ in addition to the usual simple pole.

Projection of the correlation function onto the Jordan chain.   Let the "source" and "detector" vectors in Liouville space be

$$
|B\rangle\rangle \equiv |\rho_{\rm ss} J_+\rangle\rangle, \qquad \langle\langle A| \equiv \langle\langle J_-|,
\tag{A.13}
$$

so that Eq. (A.10) becomes

$$
S(\omega) = \frac{1}{\pi} \Re \, \langle\langle A|(i\omega - \mathcal{L})^{-1}|B\rangle\rangle.
\tag{A.14}
$$

Assume the Jordan block is spanned by a generalized right eigenbasis $\{|r_0\rangle\rangle, |r_1\rangle\rangle\}$ and left eigenbasis $\{\langle\langle \ell_0|, \langle\langle \ell_1|\}$ satisfying

$$
\begin{aligned}
\mathcal{L}|r_0\rangle\rangle &= \lambda_0 |r_0\rangle\rangle, & \mathcal{L}|r_1\rangle\rangle &= \lambda_0 |r_1\rangle\rangle + |r_0\rangle\rangle, \\
\langle\langle \ell_0|\mathcal{L} &= \lambda_0 \langle\langle \ell_0|, & \langle\langle \ell_1|\mathcal{L} &= \lambda_0 \langle\langle \ell_1| + \langle\langle \ell_0|.
\end{aligned}
\tag{A.15}
$$

A convenient normalization is $\langle\langle \ell_i | r_j \rangle\rangle = \delta_{ij}$ for $i, j \in \{0, 1\}$. In this basis one may represent

$$
\mathbb{I}_{\rm sub} = |r_0\rangle\rangle\langle\langle \ell_0| + |r_1\rangle\rangle\langle\langle \ell_1|, \qquad N = |r_0\rangle\rangle\langle\langle \ell_1|.
\tag{A.16}
$$

Inserting Eq. (A.12) into Eq. (A.14) and retaining only the Jordan-block contribution yields

$$
\langle\langle A|(i\omega - \mathcal{L})^{-1}|B\rangle\rangle \simeq \frac{\alpha}{i\omega - \lambda_0} + \frac{\beta}{(i\omega - \lambda_0)^2},
\tag{A.17}
$$

with coefficients determined by overlaps with the Jordan chain,

$$
\alpha = \langle\langle A|r_0\rangle\rangle\langle\langle \ell_0|B\rangle\rangle + \langle\langle A|r_1\rangle\rangle\langle\langle \ell_1|B\rangle\rangle, \qquad \beta = \langle\langle A|r_0\rangle\rangle\langle\langle \ell_1|B\rangle\rangle.
\tag{A.18}
$$

Thus, the emission spectrum near the defective mode is controlled by a simple-pole term (α) and a second-order-pole term (β). Importantly, *both poles occur at the same complex frequency* λ_0, hence they share a common linewidth.

Real-frequency line shape: Lorentzian + super-Lorentzian.   Write the defective eigenvalue as

$$
\lambda_0 = -\gamma + i\omega_0, \qquad \gamma > 0,
\tag{A.19}
$$

and define $\Delta \equiv \omega - \omega_0$. Then

$$
i\omega - \lambda_0 = \gamma + i\Delta.
\tag{A.20}
$$

Using

$$
\Re \frac{1}{\gamma + i\Delta} = \frac{\gamma}{\Delta^2 + \gamma^2}, \qquad \Re \frac{1}{(\gamma + i\Delta)^2} = \frac{\gamma^2 - \Delta^2}{(\Delta^2 + \gamma^2)^2},
\tag{A.21}
$$

Eq. (A.17) gives the standard decomposition

$$S(\omega) \simeq \frac{1}{\pi} \left[a\, \frac{1}{\Delta^2 + \gamma^2} + b\, \frac{\gamma^2 - \Delta^2}{(\Delta^2 + \gamma^2)^2} \right], \tag{A.22}$$

where the real amplitudes a and b depend on the overlaps in Eq. (A.18). (Any overall factor of γ can be absorbed into a; we adopt the convention used in the main text.) The first term is a Lorentzian peak (simple pole), while the second is the *super-Lorentzian* contribution (second-order pole), which is the analytic fingerprint of a Jordan block.

References

[1] T. Kato, *Perturbation Theory for Linear Operators*, Springer, Berlin, Heidelberg, Reprint of the 1980 edition (first edition 1966) (1995).

[2] S. H. Weintraub, *Jordan Canonical Form: Application to Differential Equations*, Springer Cham, ISBN 978-3-031-01267-9, doi:https://doi.org/10.1007/978-3-031-02395-8 (2022).

[3] M. V. Berry, *Physics of nonhermitian degeneracies*, Czechoslovak Journal of Physics **54**(10), 1039 (2004), doi:10.1023/B:CJOP.0000044002.05657.04.

[4] I. Rotter, *A non-hermitian hamilton operator and the physics of open quantum systems*, Journal of Physics A: Mathematical and Theoretical **42**(15), 153001 (2009), doi:10.1088/1751-8113/42/15/153001.

[5] W. D. Heiss, *The physics of exceptional points*, Journal of Physics A: Mathematical and Theoretical **45**(44), 444016 (2012), doi:10.1088/1751-8113/45/44/444016.

[6] W. D. Heiss and A. L. Sannino, *Avoided level crossing and exceptional points*, Journal of Physics A: Mathematical and General **23**(7), 1167 (1990), doi:10.1088/0305-4470/23/7/022.

[7] P. Cejnar, S. Heinze and M. Macek, *Coulomb analogy for non-hermitian degeneracies near quantum phase transitions*, Phys. Rev. Lett. **99**, 100601 (2007), doi:10.1103/PhysRevLett.99.100601.

[8] J. González and R. A. Molina, *Macroscopic degeneracy of zero-mode rotating surface states in 3d dirac and weyl semimetals under radiation*, Phys. Rev. Lett. **116**, 156803 (2016), doi:10.1103/PhysRevLett.116.156803.

[9] P. San-Jose, J. Cayao, E. Prada and R. Aguado, *Majorana bound states from exceptional points in non-topological superconductors*, Scientific Reports **6**(1), 21427 (2016), doi:10.1038/srep21427.

[10] J. González and R. A. Molina, *Topological protection from exceptional points in weyl and nodal-line semimetals*, Phys. Rev. B **96**, 045437 (2017), doi:10.1103/PhysRevB.96.045437.

[11] Z. Gong, Y. Ashida, K. Kawabata, K. Takasan, S. Higashikawa and M. Ueda, *Topological phases of non-hermitian systems*, Phys. Rev. X **8**, 031079 (2018), doi:10.1103/PhysRevX.8.031079.

[12] R. A. Molina and J. González, *Surface and 3d quantum hall effects from engineering of exceptional points in nodal-line semimetals*, Phys. Rev. Lett. **120**, 146601 (2018), doi:10.1103/PhysRevLett.120.146601.

[13] E. J. Bergholtz, J. C. Budich and F. K. Kunst, *Exceptional topology of non-hermitian systems*, Rev. Mod. Phys. **93**, 015005 (2021), doi:10.1103/RevModPhys.93.015005.

[14] S. Klaiman, U. Günther and N. Moiseyev, *Visualization of branch points in $\mathcal{PT}$-symmetric waveguides*, Phys. Rev. Lett. **101**, 080402 (2008), doi:10.1103/PhysRevLett.101.080402.

[15] B. Zhen, C. W. Hsu, Y. Igarashi, L. Lu, I. Kaminer, A. Pick, S.-L. Chua, J. D. Joannopoulos and M. Soljačić, *Spawning rings of exceptional points out of dirac cones*, Nature **525**(7569), 354 (2015), doi:10.1038/nature14889.

[16] M.-A. Miri and A. Alù, *Exceptional points in optics and photonics*, Science **363**(6422), eaar7709 (2019), doi:10.1126/science.aar7709.

[17] F. Minganti, A. Miranowicz, R. W. Chhajlany and F. Nori, *Quantum exceptional points of non-hermitian hamiltonians and liouvillians: The effects of quantum jumps*, Physical Review A **100**, 062131 (2019), doi:10.1103/PhysRevA.100.062131.

[18] F. Minganti, A. Miranowicz, R. W. Chhajlany, I. I. Arkhipov and F. Nori, *Hybrid-liouvillian formalism connecting exceptional points of non-hermitian hamiltonians and liouvillians via postselection of quantum trajectories*, Physical Review A **101**, 062112 (2020), doi:10.1103/PhysRevA.101.062112.

[19] I. I. Arkhipov, A. Miranowicz, F. Minganti and F. Nori, *Quantum and semiclassical exceptional points of a linear system of coupled cavities with losses and gain within the scully-lamb laser theory*, Physical Review A **101**, 013812 (2020), doi:10.1103/PhysRevA.101.013812.

[20] I. I. Arkhipov, A. Miranowicz, F. Minganti and F. Nori, *Liouvillian exceptional points of any order in dissipative linear bosonic systems: Coherence functions and switching between $\mathcal{PT}$ and anti-$\mathcal{PT}$ symmetries*, Physical Review A **102**, 033715 (2020), doi:10.1103/PhysRevA.102.033715.

[21] K. Sun and W. Yi, *Encircling the liouvillian exceptional points: a brief review*, AAPPS Bulletin **34**(1), 1 (2024), doi:10.1007/s43673-024-00129-3.

[22] M. Naghiloo, M. Abbasi, Y. N. Joglekar and K. W. Murch, *Quantum state tomography across the exceptional point in a single dissipative qubit*, Nature Physics **15**(12), 1232 (2019), doi:10.1038/s41567-019-0652-z.

[23] A. Hashemi, K. Busch, D. N. Christodoulides, S. K. Ozdemir and R. El-Ganainy, *Linear response theory of open systems with exceptional points*, Nature Communications **13**(1), 3281 (2022), doi:10.1038/s41467-022-30715-8.

[24] S. Bid and H. Schomerus, *Uniform response theory of non-hermitian systems: Non-hermitian physics beyond the exceptional point*, Phys. Rev. Res. **7**, 023062 (2025), doi:10.1103/PhysRevResearch.7.023062.

[25] L. Simonson, S. K. Ozdemir, A. Eisfeld, A. Metelmann and R. El-Ganainy, *Nonuniversality of quantum noise in optical amplifiers operating at exceptional points*, Phys. Rev. Res. **4**, 033226 (2022), doi:10.1103/PhysRevResearch.4.033226.

[26] J. Kullig, J. Wiersig and H. Schomerus, *Generalized petermann factor of non-hermitian systems at exceptional points*, Phys. Rev. Res. **7**, 043246 (2025), doi:10.1103/5sfv-54h2.

[27] A. Rubio-García, A. L. Corps, A. Relaño, R. A. Molina, F. Pérez-Bernal, J. E. García-Ramos and J. Dukelsky, *Exceptional spectral phase in a dissipative collective spin model*, Physical Review A **106**, L010201 (2022), doi:10.1103/PhysRevA.106.L010201.

[28] C. S. Muñoz, B. Buča, J. Tindall, A. González-Tudela, D. Jaksch and D. Porras, *Symmetries and conservation laws in quantum trajectories: Dissipative freezing*, Physical Review A **100**, 042113 (2019), doi:10.1103/PhysRevA.100.042113.

[29] G. Lindblad, *On the generators of quantum dynamical semigroups*, Communications in Mathematical Physics **48**(2), 119 (1976), doi:10.1007/BF01608499.

[30] V. Gorini, A. Kossakowski and E. C. G. Sudarshan, *Completely positive dynamical semigroups of n-level systems*, Journal of Mathematical Physics **17**(5), 821 (1976), doi:10.1063/1.522979.

[31] P. Ribeiro and T. Prosen, *Integrable quantum dynamics of open collective spin models*, Phys. Rev. Lett. **122**, 010401 (2019), doi:10.1103/PhysRevLett.122.010401.

[32] R. H. Dicke, *Coherence in spontaneous radiation processes*, Physical Review **93**, 99 (1954), doi:10.1103/PhysRev.93.99.

[33] M. Gross and S. Haroche, *Superradiance: An essay on the theory of collective spontaneous emission*, Physics Reports **93**(5), 301 (1982), doi:10.1016/0370-1573(82)90102-8.

[34] C. W. Gardiner and P. Zoller, *Quantum Noise: A Handbook of Markovian and Non-Markovian Quantum Stochastic Methods with Applications to Quantum Optics*, Springer, Berlin, Heidelberg, 3 edn., ISBN 978-3-540-22301-6 (2004).

[35] J. Fransson, O. Eriksson and A. V. Balatsky, *Theory of spin-polarized scanning tunneling microscopy applied to local spins*, Phys. Rev. B **81**, 115454 (2010), doi:10.1103/PhysRevB.81.115454.

[36] F. Delgado, J. J. Palacios and J. Fernández-Rossier, *Spin-transfer torque on a single magnetic adatom*, Phys. Rev. Lett. **104**, 026601 (2010), doi:10.1103/PhysRevLett.104.026601.

[37] S. Baumann, W. Paul, T. Choi, C. P. Lutz, A. Ardavan and A. J. Heinrich, *Electron paramagnetic resonance of individual atoms on a surface*, Science **350**(6259), 417 (2015), doi:10.1126/science.aac8703.

[38] H. J. Carmichael, *Statistical Methods in Quantum Optics 1: Master Equations and Fokker-Planck Equations*, Springer, Berlin, Heidelberg, ISBN 978-3-540-54882-9 (1999).

[39] J. Fransson, *Theory of spin-polarized scanning tunneling microscopy and spectroscopy of single magnetic atoms*, Physical Review B **81**, 115454 (2010), doi:10.1103/PhysRevB.81.115454.

[40] G. Schwarz, *Estimating the Dimension of a Model*, The Annals of Statistics **6**(2), 461 (1978), doi:10.1214/aos/1176344136.

[41] K. P. Burnham and D. R. Anderson, *Model Selection and Multimodel Inference: A Practical Information-Theoretic Approach*, Springer, New York, 2 edn., ISBN 978-0-387-95364-9 (2002).

[42] M. Am-Shallem, A. Levy, I. Schaefer and R. Kosloff, *Three approaches for representing lindblad dynamics by a matrix-vector notation*, arXiv:1510.08634 [quant-ph] (2015), ArXiv preprint.

[43] B. Buča and T. Prosen, *Exact non-equilibrium steady state of a strongly driven open xxz chain*, Physical Review Letters **120**, 067201 (2018), doi:10.1103/PhysRevLett.120.067201.

[44] J. a. S. Ferreira and P. Ribeiro, *Lipkin-meshkov-glick model with markovian dissipation: A description of a collective spin on a metallic surface*, Phys. Rev. B **100**, 184422 (2019), doi:10.1103/PhysRevB.100.184422.

[45] P. Cejnar, P. Stránský, M. Macek and M. Kloc, *Excited-state quantum phase transitions*, Journal of Physics A: Mathematical and Theoretical **54**(13), 133001 (2021), doi:10.1088/1751-8121/abdfe8.